processes

MDPI

Article

Validation of Fluid Flow Speed Behavior in Capillary Microchannels Using Additive Manufacturing (SLA Technology)

Victor H. Cabrera-Moreta [1,2,*], Jasmina Casals-Terré [1] and Erick Salguero [2]

[1] Laboratory of Microsystems and Nanotechnology, Mechanical Engineering Department, Polytechnic University of Catalonia (UPC), Colom Street 11, 08222 Terrassa, Spain; jasmina.casals@upc.edu
[2] Mechanical Engineering Department, Universidad Politécnica Salesiana, Quito 170517, Ecuador; esalgueror@est.ups.edu.ec
* Correspondence: victor.cabrera.moreta@upc.edu or vcabrera@ups.edu.ec

Abstract: This research explores fluid flow speed behavior in capillary channels using additive manufacturing, focusing on stereolithography (SLA). It aims to validate microchannels fabricated through SLA for desired fluid flow characteristics, particularly capillary-driven flow. The methodology involves designing, fabricating, and characterizing microchannels via SLA, with improvements such as an air-cleaning step facilitating the production of microchannels ranging from 300 to 1000 µm. Experimental validation assesses fluid flow speed behavior across channels of varying dimensions, evaluating the impact of channel geometry, surface roughness, and manufacturing parameters. The findings affirm the feasibility and efficacy of SLA in producing microchannels with consistent and predictable fluid flow behavior between 300 to 800 µm. This study contributes insights into microfluidic device fabrication techniques and enhances the understanding of fluid dynamics in capillary-driven systems. Overall, it underscores the potential of additive manufacturing, specifically SLA, in offering cost-effective and scalable solutions for microfluidic applications. The validated fluid flow speed behavior in capillary channels suggests new avenues for developing innovative microfluidic devices with improved performance and functionality, marking a significant advancement in the field.

Keywords: additive manufacturing; stereolithography (SLA); microchannels; capillary-driven

check for updates

Citation: Cabrera-Moreta, V.H.; Casals-Terré, J.; Salguero, E. Validation of Fluid Flow Speed Behavior in Capillary Microchannels Using Additive Manufacturing (SLA Technology). *Processes* **2024**, *12*, 1066. https://doi.org/10.3390/pr12061066

Academic Editors: Guoqing Zhang, Zejia Zhao and Wai Sze Yip

Received: 3 April 2024
Revised: 30 April 2024
Accepted: 7 May 2024
Published: 23 May 2024

Copyright: © 2024 by the authors. Licensee MDPI, Basel, Switzerland. This article is an open access article distributed under the terms and conditions of the Creative Commons Attribution (CC BY) license (https://creativecommons.org/licenses/by/4.0/).

1. Introduction

Figure 1 demonstrates the exponential growth of additive manufacturing and 3D printing in microfluidics over the past two decades [1]. This trend highlights the increasing recognition of 3D printing as a powerful tool in microfluidic research, enabling the fabrication of intricate devices with tailored designs and functionalities. This evolution promises to revolutionize microfluidic experimentation and applications, ushering in a new era of innovation and discovery in the field [2].

Additive manufacturing has emerged as an appealing option for producing microfluidic chips across various applications. Compared to traditional methods like soft lithography, additive manufacturing offers a straightforward, rapid, and cost-effective approach to creating microstructures. One of its key advantages lies in the accessibility and affordability of the necessary equipment, making it feasible for both industry and research laboratories. Over recent years, a range of rapid prototyping methods, including 3D printing, have surfaced as invaluable tools for developing microfluidic devices [1]. Figure 2 provides an overview of the additive manufacturing technologies currently accessible in the market.

Despite the array of additive manufacturing technologies available, research will primarily concentrate on SLA, Polyjet (MultiJet), or FDM due to their accessibility and cost-effectiveness. These technologies will be compared based on their respective advantages and disadvantages within the field. Table 1 presents a condensed summary of the most pertinent information concerning these listed technologies [2–6].

Table 1 highlights crucial characteristics for selecting the optimal technology for future micromixers. The initial cost is a major consideration, with SLA offering the lowest startup expense. Resolution varies among technologies but is generally acceptable for microdevices. Polyjet and FDM have an advantage over SLA as they do not require post-processing [2].

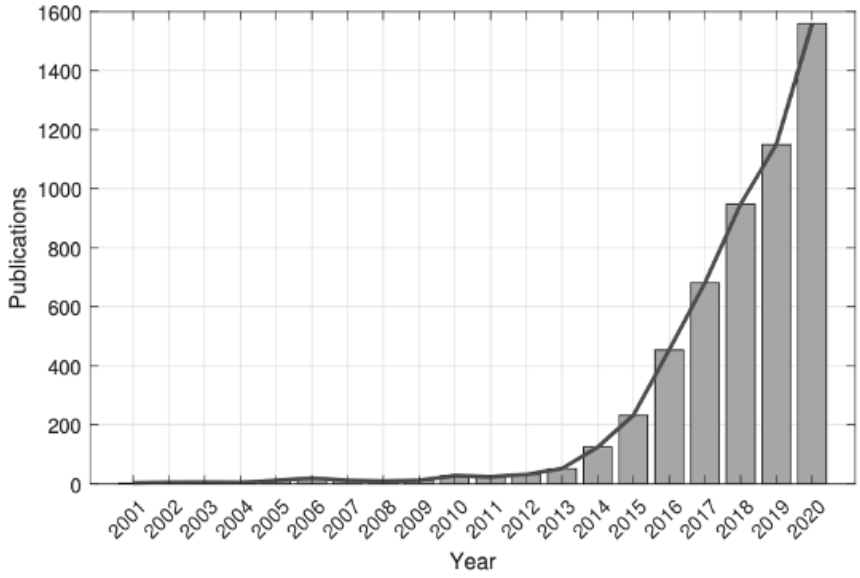

Figure 1. Trends of 3D printing, microfluidic, and additive manufacturing published articles [2].

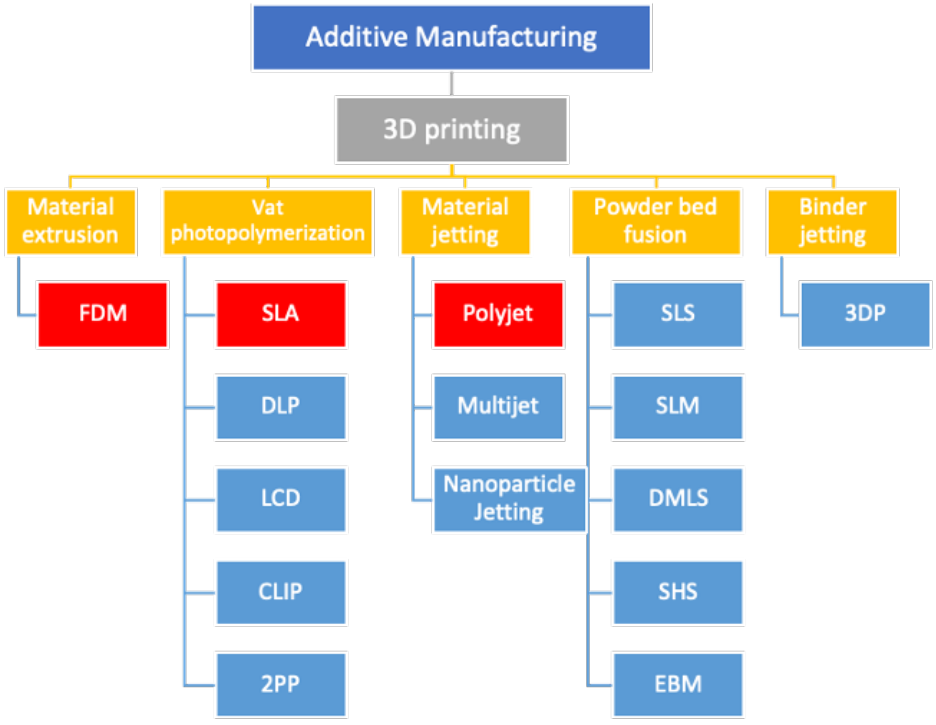

Figure 2. 3D printing categories and technologies [2,3].

All technologies exhibit an acceptable building rate, significantly reducing manufacturing time to a few hours for final prototypes compared to traditional methods. Ongoing research employs additive manufacturing for microfluidic devices, addressing manufacturing restrictions to broaden application possibilities. Challenges include improving surface quality, post-processing, and reducing device costs [7,8].

SLA printing technology, known for its cost-effectiveness and reasonable resolution (ranging from 0.025 to 0.1 mm), stands out as one of the most utilized methods in mi-

crofabrication. Post-processing typically involves washing with isopropanol followed by UV post-curing [9], though this step may be viewed as a limitation of the process. The specific time and configuration parameters for post-processing vary depending on the application, representing an important yet uncertain parameter to define for the current study. Given the significance of SLA technology in microdevice manufacturing, Table 2 provides a summarized literature review of research utilizing SLA as a manufacturing process, including miniaturized SLA arrays [1,10,11].

Table 1. 3D printed mixers [2–6].

Additive Manufacturing Technology	SLA (Stereolithography)	Polyjet	FDM (Fused Deposition Modeling)
Cost of main equipment	$2500–$3400	$60,000–$300,000	$1000
Post-processing equipment cost	Wash: $499 Cure: $699	None	None
Material required	Resin Consumable resin tank Isopropyl Alcohol	Liquid photopolymer Caustic soda solution	PLA
Layer print height	0.025 mm 0.05 mm 0.100 mm	High Quality High Mix High Speed	0.15 mm 0.20 mm 0.30 mm
Build rate	0.18–1.16	0.10–0.19	0.06–0.33

Table 2. 3D-printed SLA devices.

Active method	Channel range	Application	Material	Ref.	Year
Syringe pump	100–500 µm	Microfluidic droplet	Grey Resin	[12]	2021
Syringe pump	280–310 µm	SLA 3D printed droplet generators	Clear Resin	[1]	2021
Mini centrifuge	1–2 mm	Platform for multiplexed molecular detection of SARS-CoV-2.	Clear Resin	[13]	2021
Syringe pump	1000 µm	Laboratory experiments	Clear Resin	[14]	2020
Syringe pump	1.58 mm	Controlled Microdroplets	Clear Resin	[15]	2019
Syringe pump	100–500 µm	Modular microfluidic for emulsion droplets	Curable polymer	[16]	2019

This research endeavors to investigate the feasibility of utilizing additive manufacturing, specifically SLA, to fabricate microchannels for determining fluid velocity. By leveraging insights gained from previous micromixer devices, the study aims to delineate its scope effectively.

Early studies primarily examined flows within straight pipes of varying geometries and used active methods to operate them, such as syringe pumps. Interest then shifted to investigating flow behavior in capillary tubes under microgravity conditions. Recent research has focused on hydrodynamics and mass transfer in microchannels with diameters <1 mm, crucial for bio- and micro-fluidic applications. Experimental parameters include inlet geometry, cross-sections, flow rates, and fluid properties. Studies typically concentrate on low flow velocities dominated by surface forces, resulting in intermittent

flow patterns [17]. Researchers have explored various miniature geometries, including straight channels with circular or rectangular cross-sections. These studies have shown that different geometries exhibit distinct flow characteristics and performance. For instance, straight channels with rectangular cross-sections may offer advantages over those with circular cross-sections in terms of fluid dynamics and mass transfer efficiency [18]. An application could involve utilizing capillary-driven flow in microchannels for precise fluid control in lab-on-a-chip devices, benefiting medical diagnostics and chemical analysis [17].

Surface roughness is a factor that can alter fluid behavior within microchannels. The impact of this factor could change the characteristics of a material from hydrophobic to hydrophilic [19,20]. However, for this study, the surface of the resin used was not affected. The material exhibited hydrophilic behavior according to the results obtained.

The ultimate objective is to develop a passive microfluidic device suitable for deployment as a mobile lab-on-chip, obviating the need for an external power source. This endeavor requires an alternative manufacturing approach capable of producing intricate geometries to exploit the laminar flow behavior inherent in microdevices. SLA technology emerges as a promising method due to its precision and capability to achieve the desired outcomes. Ensuring compact dimensions is paramount to facilitate portability and ease of handling for the device.

2. Materials and Methods

2.1. Device Printing Process

The traditional and recommended SLA 3D printing process includes four main steps: digital design, printing, washing, and curing [15]. However, microchannels under 400 µm the channels showed a material stagnation. As a result, an improvement in the process was added.

The recommended printing workflow is shown in Figure 3. The process includes an air-cleaning step. The effectiveness of the process variation is evident in the results, as clear channels up to 300 µm and beyond are obtained.

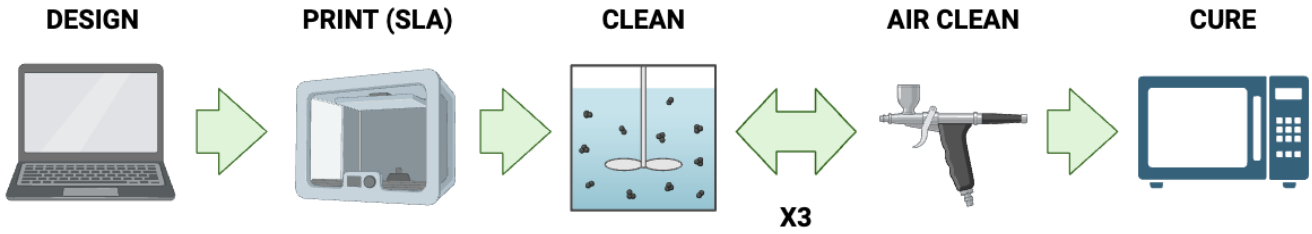

Figure 3. Optimized 3D printing process.

Design: The initial step involves creating a 3D model of the mixer using parametric software, specifically SOLIDWORKS 2024. Once the design is complete, it is exported as a stereolithography file (STL) for further processing, with a straight channel of 25 mm in length and square section of 300 to 1000 µm. Figure 4 shows an example of the designed device. Printing: The FORM 3+ printer, manufactured by Formlabs, is used for this stage. SLA technology is employed to manufacture the models, with a printing resolution set as an adaptative resolution. The adaptive printing method adapts each layer into the proper resolution from 25 to 100 µm). The printer has a maximum build dimension of 145 × 145 mm flat and 185 mm height. Devices are printed using CLEAR RESIN (by Formlabs Inc., Somerville, MA, USA) chosen for its ability to provide clear images of the process.

Cleaning: Post-printing, a crucial cleaning process using isopropyl alcohol, is undertaken to remove any uncured resin that could potentially clog the channels. An automated washer, the FORMWASH, is employed for this task.

Air Cleaning: An air-cleaning process is incorporated to ensure thorough cleaning. The washer conducts a 5-minute wash cycle followed by air cleaning at 4 psi pressure, repeated three times. After this, the device undergoes final curing. This stage allows for the obtaining of a clean and more accurate channel size before UV exposure. The cleaning regimen consisted of intervals set every 5 min for a total of 3 iterations. Despite conducting additional cycles beyond the prescribed 3, discernible enhancements in the outcomes were not observed. It was elucidated that the third iteration of air cleaning sufficed in eliminating all residual uncured resin.

Curing: The curing process takes place in a FORMCURE curing chamber, where the device is exposed to ultraviolet rays. Curing occurs at 60° for a duration of 15 min to ensure optimal strength and stability of the model. To prevent device deformation due to heat and UV rays, tempered glass sheets were used to cover the devices.

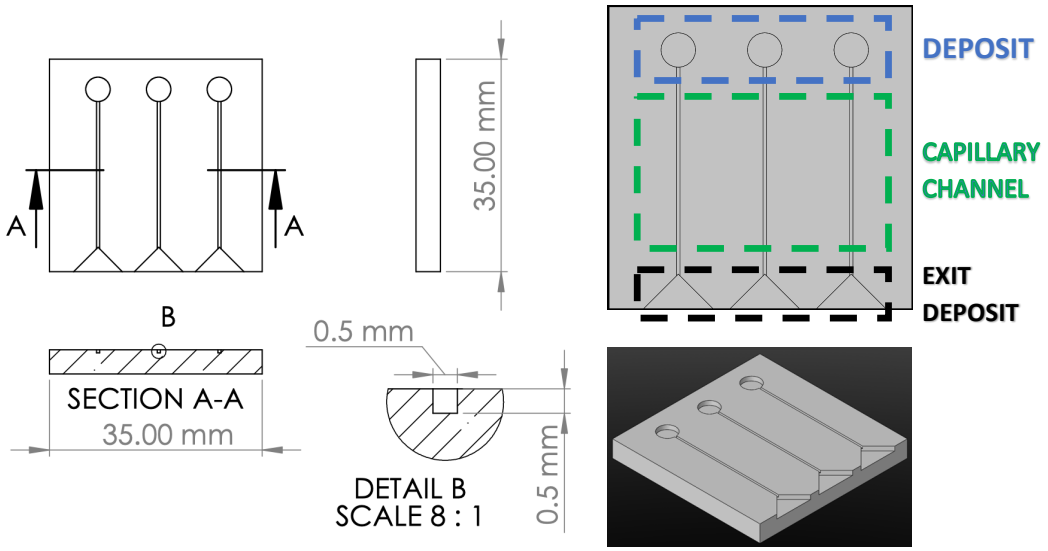

Figure 4. Reference images of test devices.

2.2. Device Setup and Data Collect

2.2.1. Device Preparation

The device is designed with a closed channel to achieve optimal capillary flow. However, additive SLA technology does not allow for the fabrication of closed channels. Therefore, open channels were designed, as shown in Figure 4, where side walls and the base were fabricated. The channel was closed by adding the top wall using a specialized hydrophilic adhesive to enhance capillary flow. This adhesive is uniformly applied to the device surfaces, promoting optimal wetting of the channels and facilitating smooth fluid flow. Specification: 3M 9984 Diagnostic Microfluidic Surfactant Free Hydrophilic Film.

The prepared device undergoes thorough cleaning with high-purity distilled water (Grade 0) to eliminate any lingering contaminants or particles. Following this, it is dried using a controlled stream of compressed air at 5 psi. This meticulous cleaning and drying process is conducted before each new experiment to ensure consistent and reliable outcomes.

2.2.2. Experimental Setup

Before commencing each experiment, the microdevice is carefully placed on a precision-leveled platform to mitigate any potential disruptions resulting from tilting or uneven surfaces. The initial experiments, where the stabilization process on the platform was not considered, lacked stability and consistency in the values obtained. Upon leveling the platform using leveling tools, the results began to exhibit greater coherence and repeatability. These results were not included in the research as they were considered a minor factor.

A precisely measured 20 µL volume of high-purity distilled water (Grade 0) is dispensed into the reservoir of each channel using a calibrated pipette, as illustrated in Figure 4. This distilled water is pre-prepared with a biocompatible vegetable dye to facilitate the visualization of fluid flow. Upon dispensing into the reservoir, the water is driven through the channel by capillary force.

2.3. Video and Image Processing

Image and Video Capture: Utilizing a USB digital microscope (Dino-Lite Digital Microscope AF4515ZTL, AnMo Electronics Corporation, Taipei, Taiwan), high-resolution images and videos were captured. To optimize illumination for image and video capture, a smartphone with a white light screen was strategically positioned beneath the device (Figure 5b).

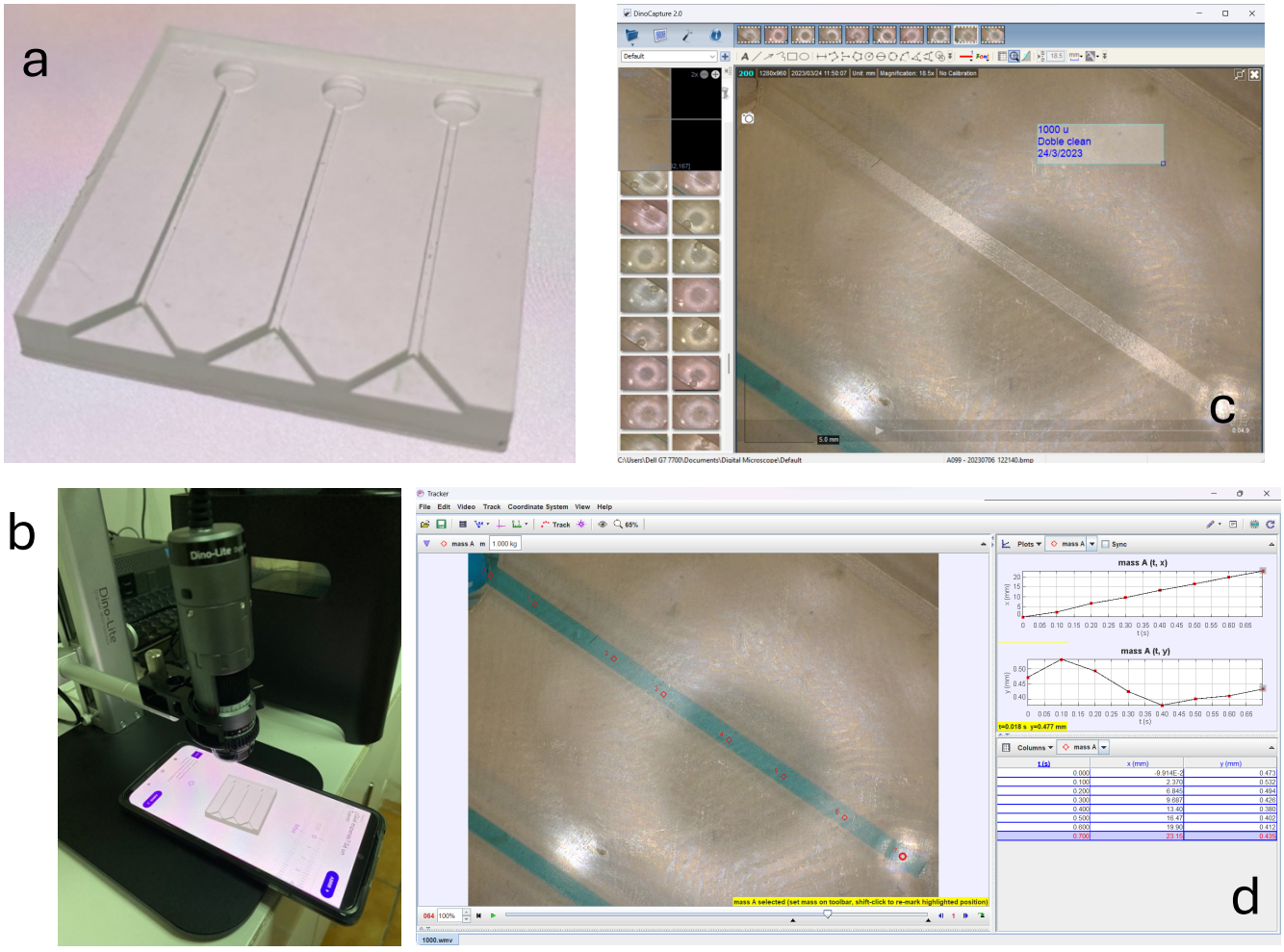

Figure 5. Data analysis process (**a**) prepare device (**b**) setup of experiment (**c**) capture images with microscope (**d**) obtain data.

Software Utilization: The DINO CAPTURE 2.0 software was employed to save image and video files, ensuring standardized and organized data storage. Additionally, it facilitated the real-time observation of the microfluidic processes.

Channel Size: To ascertain the actual dimensions of the channels, a profilometer (Bruker brand, model Dektak XT) was utilized. Validation was conducted through image correlation with the Dino-Lite Digital Microscope (AnMo Electronics Corporation, Taipei, Taiwan).

Angle Measurements of the Drop Over Surfaces (Resin and Adhesive): To precisely measure contact angles, we employed a USB microscope for image capture, then conducted a thorough analysis using the freely available image processing software, IMAGE J (Version 1.54i). The revealed contact angles averaged 49.2° with a standard deviation of 2.93°. Additionally, we determined that the static contact angle on the adhesive used in our study averaged 54.8° with a standard deviation of 3.84°. These measurements offer valuable insights into the wetting behavior of various materials within our microdevice, providing essential data for assessing fluid dynamics and surface interactions. The data were utilized for calculations in the article.

2.4. Data Analysis

Velocity Measurements: The velocity data were derived from the videos captured using TRACKER (version 6). Velocity analysis was conducted using image and video analysis techniques. The experiment was recorded using video and image processing. The data were analyzed using the software TRACKER. Image processing was carried out over a 0.1-s interval, during which the position of fluid was compared to its previous position. This allowed for data tabulation and the establishment of flow velocity at different points. This allowed for the computation of fluid velocities within the microchannels.

Graphical Representation: MATLAB R2023a was utilized for data processing and generating graphical representations. Graphs and figures were created to illustrate the experimental findings, facilitating data interpretation and comparison.

By following this refined methodology, we ensure precise device preparation, optimal surface treatment, controlled experimental setup, precise data acquisition, and analysis in our capillary-driven microdevice mixer study, all of which are essential for accurate and replicable results in capillary-driven microdevice mixing studies. The combination of advanced imaging techniques and powerful software tools enabled the accurate quantification of contact angles, fluid velocities, color changes, and mixing patterns, providing a thorough understanding of the device's performance and its comparison with simulation data.

2.5. Govern Equations

2.5.1. Capillary Pressure

$$\Delta P = \gamma \left(\frac{cos\left(\theta_{left}\right) + cos\left(\theta_{right}\right)}{w} + \frac{cos\left(\theta_{top}\right) + cos(\theta_{bottom})}{h} \right) \quad (1)$$

ΔP—Capillary Pressure.
$cos\left(\theta_{top}\right)$—contact angle with adhesive = 54.8°.
$cos\left(\theta_{left}\right)$, $cos\left(\theta_{right}\right)$, $cos(\theta_{bottom})$—contact angle with resin = 49.2°.
w—channel depth = 300 µm to 1000 µm .
h—channel width = 300 µm to 1000 µm.
γ—surface tension of liquid [N/m] = 0.07 N/m N/m = 70 mN/m.

2.5.2. Fluid Flow

$$Q = \Delta P \frac{{h_0}^3 w}{12 \mu L} \gamma \left[1 - 0.63 \frac{h_0}{w} \right] \quad (2)$$

ΔP—Capillary Pressure.
h_0—channel depth = 300 µm to 1000 µm.
w—channel width = 300 µm to 1000 µm.
L—channel length = 25 mm.
γ—surface tension of liquid [N/m] = 0.07 N/m N/m = 70 mN/m.
μ—Kinematic viscosity of water = 8.9×10^{-4} Pa s.

2.5.3. Velocity

$$V = \frac{Q}{A} \tag{3}$$

Q—Fluid flow.
A—Channel section = width and depth size between 300 µm to 1000 µm.

3. Results

3.1. Printed Results

Following a series of iterative printing tests and refinements, we present the finalized design of the proposed device, as depicted in Figures 6 and 7. This culmination of multiple printing experiments represents our commitment to achieving the optimal configuration and functionality of the device, ensuring that it meets the highest standards of performance and precision.

The enhancements made to the printing process yielded significant results. Initially, as depicted in Figure 6, resin stagnation was noticeable within the channels, particularly those under 500 µm in width. The printing method suggested by the provider proved insufficient in achieving the desired channel specifications, resulting in resin stagnation that impeded fluid flow. Following the implementation of an air-cleaning process, notable improvements were observed (Figure 7). Channels ranging from 300 µm to 1000 µm in width were successfully produced. However, further investigation revealed that 400 µm channels represent the smallest size attainable for obstruction-free applications. Air cleaning proved instrumental in facilitating the creation of smaller channel sizes, ensuring smoother fluid flow. Its importance lies in its efficacy in eliminating stagnation residue introduced during the printing process.

The occurrence of channel clogging arises from the challenge of effectively removing residual resin from within the channels using current processing methods. To address this issue, we are exploring various post-processing techniques aimed at efficiently eliminating excess material. Methods such as sandblasting and utilizing alternative cleaning agents besides isopropyl alcohol are being considered to be potential solutions to mitigate this problem.

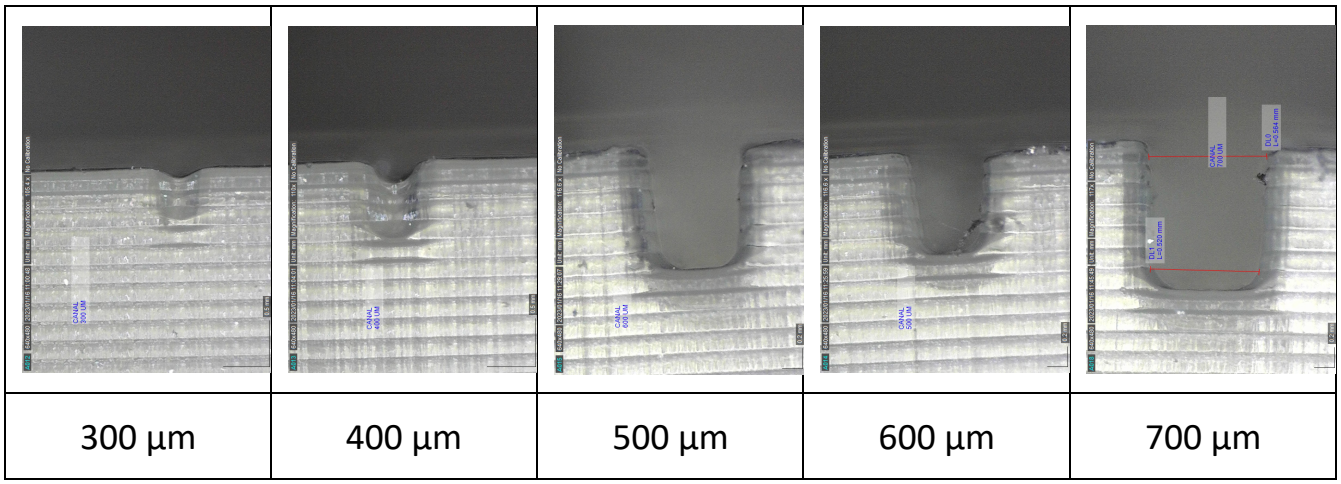

Figure 6. Printed Devices with traditional process.

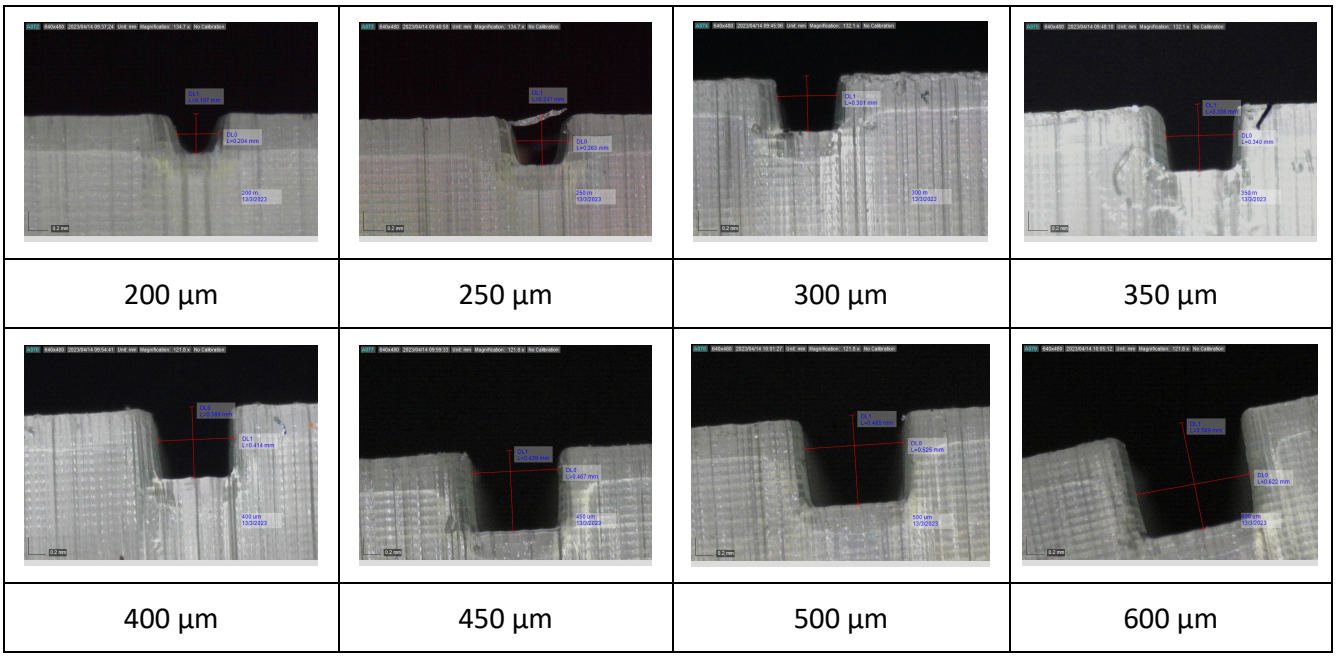

Figure 7. Printed Devices with proposed process.

The channel measurements were validated using both a USB microscope and a scanning electron microscope (SEM), each possessing the following characteristics.

Scan time: 400 s for each zone.

- Length scan: 20,000–50,000 µm.
- Scan resolution: 0.0166667–0.0462954 µm.
- Scan type: Standard.
- Needle force: 3 mg.
- Needle range scan: 1 mm.
- Needle type: radius 25 µm.
- Correction: quadratic and removal of curvature.

Figure 8 illustrates the measurement results of the obtained channels. It allows for comparison between the channel size designed using software and the size obtained after printing.

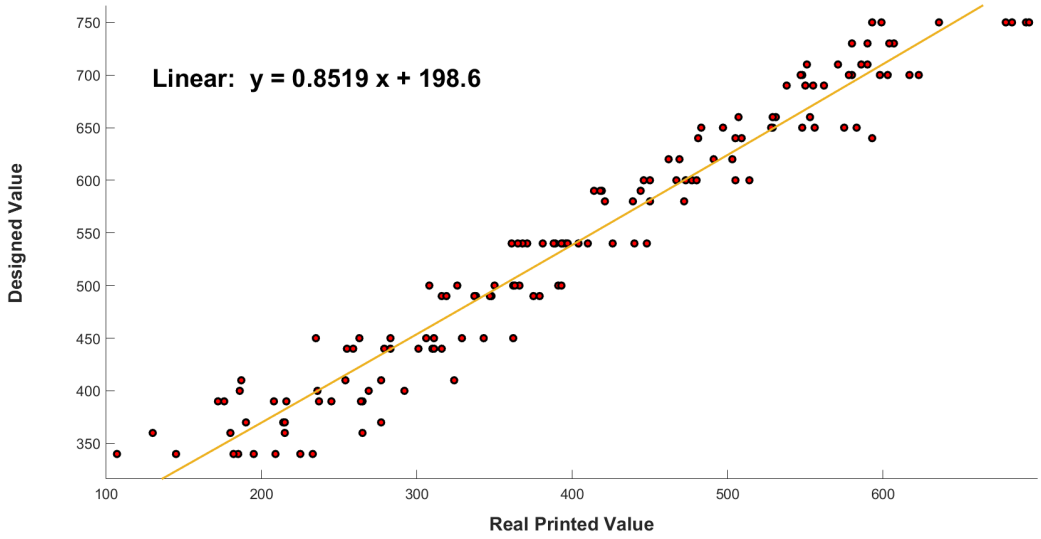

Figure 8. Printed results compared to Designed results.

In general, we can observe data dispersion across all measurements. Nevertheless, a linear relationship exists. Thus, we were able to establish the equation that enables the determination of the channel size to be designed in order to achieve a specific actual channel value.

$$y = 0.8519x + 198.6 \quad (4)$$

The correlation coefficient was established between the designed value variables compared to the actual width measurement obtained on the device after printing. The correlation coefficient was 0.9747, indicating a strong positive correlation between the two variables. Consequently, they tend to change in the same direction.

The proposed equation has been validated and is currently being utilized in devices to determine the size of channels. The variation in the proposed channel size compared to the actual size is attributed to several factors. Among the main factors is that the equipment used lacks recommendations for printing elements on a micro scale. Thus, the tolerance exhibited by the printing at channels of this size becomes evident and, therefore, warrants an adjustment.

Based on the printed devices, it was found that channels up to 150 µm wide can be printed. However, the channels are not uniform and exhibit stagnant resin. For this reason, it is recommended that channels be used between 400 and 800 µm wide to avoid resin blockage. This was verified by conducting tests with fluid through the channels. These experiments were not included in the presented results.

3.2. Velocity of the Fluid During the Experiment

Once the devices were printed and prepared for capillarity tests, velocities were measured in channels of 25 mm length and square sections ranging from 300 to 1000 µm. Throughout the channels, it was observed that the velocity maintained its stability consistently. Subsequently, velocity data for each of the channels were recorded and plotted in Figure 9.

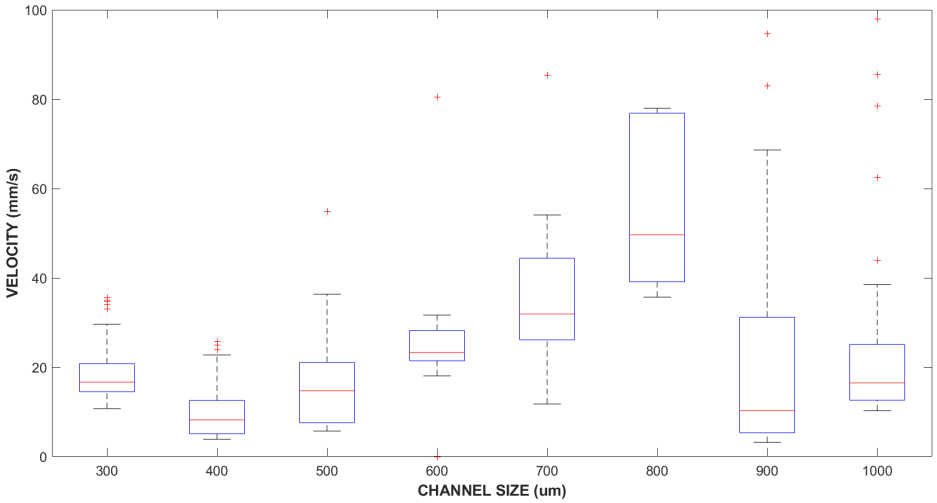

Figure 9. Boxplot of velocity (mm/s) in different channel size.

In Table 3, a summary of the data obtained from the various channels between 300 and 1000 µm is presented.

Table 3. Experimental data velocity for different channel size.

Channel Size	300	400	500	600	700	800	900	1000
Mean (mm/s)	18.62	9.24	17.77	26.89	37.75	61.16	25.53	26.32
Standard Deviation (mm/s)	6.54	4.78	14.09	18.64	22.63	33.37	34.01	24.12

Both the resin and the cover layer demonstrate hydrophilic properties, leading to enhanced fluid interaction. The larger surface area of the walls facilitates increased contact with the fluid, resulting in a greater thrust force to propel it forward. This relationship is illustrated in Figure 8, where velocity demonstrates a corresponding increase with surface area increment. However, for channels exceeding 800 µm or falling below 300 µm, additional factors influence velocity. Through our research, we have established that velocities between 400 µm and 800 µm are stable based on the data analysis.

As an experimental process, various factors, such as printing techniques and other variables, can influence the final device, leading to a degree of uncertainty in predicting the speed of future devices. While current technology may not eliminate this uncertainty, ensuring the reliability of experiments through meticulous data analysis and statistical validation enhances the confidence in the obtained results, as shown in Table 4.

Figure 10 illustrates the relationship between the calculated capillary pressure and the experimentally obtained velocity in the devices, compared with the channel size (300 µm to 1000 µm). It is evident that printing and surface roughness result in an exponential increase in velocity between 400 and 800 µm. According to previous studies, roughness smaller than the drop size generates greater surface hydrophilicity [20]. For our study, the measured roughness was 4.99 µm with a standard deviation of 0.87 µm. The roughness is much smaller than the drop size (3 mm radius). Variations in roughness could alter velocity results through the principle of capillarity [19].

Table 4. Data of capillary data for different channel sizes.

Width Height (µm)	P (Pa)	Q (mm^3/s)	V (mm/s)	V Exp (mm/s)
300	0.63149	0.0071	0.0788	0.1862
400	0.47362	0.0168	0.105	0.0924
500	0.3789	0.0328	0.1313	0.1777
600	0.31575	0.0567	0.1575	0.2689
700	0.27064	0.09	0.1838	0.3775
800	0.23681	0.1344	0.21	0.6116
900	0.2105	0.1914	0.2363	0.2553
1000	0.18945	0.2625	0.2625	0.2632

In general, this research document showcases the feasibility of utilizing additive manufacturing equipment to produce microchannels (ranging from 300 to 1000 µm) for device applications. It was possible to establish the proposed design parameters for obtaining channels of the required dimensions. Additionally, it was confirmed that the obtained channels are suitable for capillary action applications. Moreover, the study demonstrates the potential of additive manufacturing techniques in microfluidic device fabrication, highlighting their adaptability and precision in producing microstructures with specific geometrical requirements.

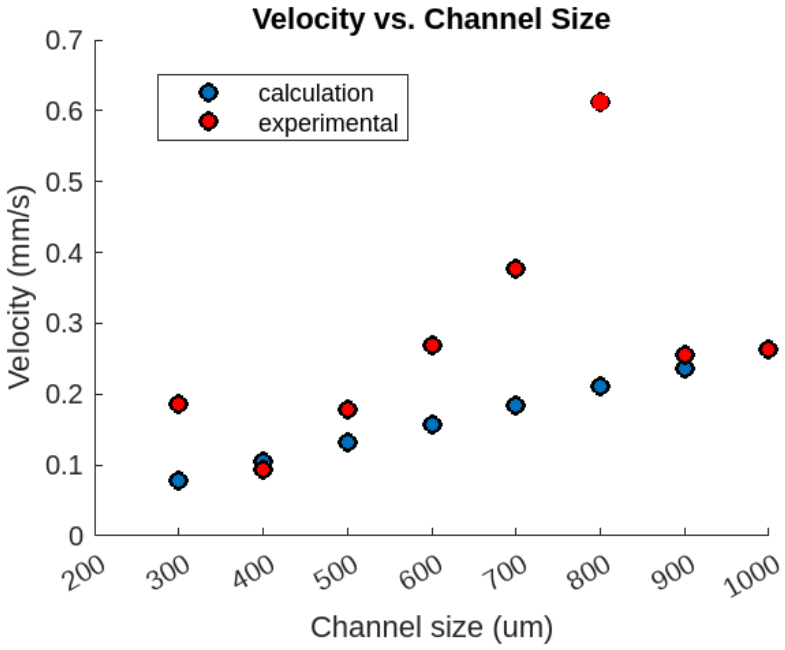

Figure 10. Comparative graph between calculation and experimental data.

4. Conclusions

It has been determined that to obtain microchannels of 300 µm or larger, a proper washing and curing process must be followed to prevent material stagnation. Adding a triple-compressed air-cleaning process at 5 bar between the washing and curing steps allows for the attainment of the expected channel dimensions.

This study successfully validated the use of stereolithography (SLA) 3D-printing technology for fabricating microchannel devices with consistent capillary-driven fluid flow behavior. The key findings showed that channels ranging from 300 to 1000 µm could be reliably produced using an optimized SLA printing process with an added air-cleaning step. The equation $y = 0.8519\ x + 198.6$ was derived to predict the actual printed channel size based on the designed dimensions, accounting for fabrication inaccuracies at the microscale.

The mean fluid velocities measured experimentally aligned well with theoretical calculations, validating the flow behavior in the printed channels. For instance, the 500 µm channel exhibited a mean velocity of 17.77 mm/s, closely matching the calculated value of 13.13 mm/s. This concordance between experimental data and theory substantiates the suitability of SLA printing for realizing precisely designed microfluidic components driven by capillary forces. Experimental data demonstrated that fluid velocities increased exponentially with larger channel sizes, reaching up to 61.16 mm/s for 800 µm channels.

According to the comparison between mean experimental velocity values and theoretical ones, there is a correlation up to the 800 µm channel. Channels ranging from 400 to 800 µm present a standard deviation between 4.78 and 33.37 mm/s. Hence, we can infer that for channels within these ranges, repeatability in results can be achieved. Channels larger than 800 µm exhibit a deviation greater than 33.37 mm/s, assuming a variation in the processes. This is because external variables such as gravity, material roughness, and channel size significantly affect the process, rendering it unpredictable.

In conclusion, this study delineates an appropriate printing and post-processing procedure that enables the production of channels from 300 µm. To obtain the desired channel values, it is important to use the determined formula to define the channel size to be designed. This could contribute to the development of future devices. Additionally, it is recommended to work with channels between 300 and 800 µm, which exhibit

stable capillary-driven fluid velocity values. This could contribute to the development of future devices.

Author Contributions: V.H.C.-M. executed the conceptualization, investigation, data analysis, manuscript preparation and wrote the original draft; J.C.-T. supervised, reviewed, and edited the manuscript. E.S. validated the manuscript. All authors have read and agreed to the published version of the manuscript.

Funding: This work is funded by the Universidad Politécnica Salesiana through Research Project (035-01-2024-01-30). Additionally, it received support from the Ministerio de Ciencia e Innovación (PID2020-114070RB-I00), the Agencia Estatal de Investigación (CPP2021-009021), and AGUAR (2021PROD00064).

Data Availability Statement: All data generated or analyzed during this study are included in this published article or available from the corresponding author upon reasonable request.

Acknowledgments: We gratefully acknowledge ESPE (Universidad de las Fuerzas Armadas) for providing facilities and resources for Scanning Electron Microscopy (SEM) microscopy, particularly Nanomaterials Characterization Laboratory Center of Nanoscience and Nanotechnology (CENCI-NAT). Special thanks to Alexis Debut. We appreciate the technical assistance of Karla Vizuete for their guidance and support during the process.

Conflicts of Interest: The authors declare no conflict of interest.

Abbreviations

The following abbreviations are used in this manuscript:

SLA	Stereolithography
FDM	Fused Deposition Modeling
UV	Ultraviolet

References

1. Bacha, T.W.; Manuguerra, D.C.; Marano, R.A.; Stanzione, J.F. Hydrophilic modification of SLA 3D printed droplet generators by photochemical grafting. *RSC Adv.* **2021**, *11*, 21745–21753. [CrossRef] [PubMed]
2. Garcia-Cardosa, M.; Granados-Ortiz, F.J.; Ortega-Casanova, J. A Review on Additive Manufacturing of Micromixing Devices. *Micromachines* **2021**, *13*, 73. [CrossRef] [PubMed]
3. Rogers, C.I.; Qaderi, K.; Woolley, A.T.; Nordin, G.P. 3D printed microfluidic devices with integrated valves. *Biomicrofluidics* **2015**, *9*, 011502. [CrossRef] [PubMed]
4. Chen, C.; Mehl, B.T.; Munshi, A.S.; Townsend, A.D.; Spence, D.M.; Martin, R.S. 3D-printed microfluidic devices: Fabrication, advantages and limitations—A mini review. *Anal. Methods* **2016**, *8*, 6005–6012. [CrossRef] [PubMed]
5. Dixit, C.K.; Kadimisetty, K.; Rusling, J. 3D-printed miniaturized fluidic tools in chemistry and biology. *TrAC Trends Anal. Chem.* **2018**, *106*, 37–52. [CrossRef] [PubMed]
6. Chen, J.V.; Dang, A.B.C.; Dang, A. Comparing cost and print time estimates for six commercially-available 3D printers obtained through slicing software for clinically relevant anatomical models. *3D Print. Med.* **2021**, *7*, 1. [CrossRef] [PubMed]
7. Shallan, A.I.; Smejkal, P.; Corban, M.; Guijt, R.M.; Breadmore, M.C. Cost-Effective Three-Dimensional Printing of Visibly Transparent Microchips within Minutes. *Anal. Chem.* **2014**, *86*, 3124–3130. [CrossRef] [PubMed]
8. Tiboni, M.; Tiboni, M.; Pierro, A.; Del Papa, M.; Sparaventi, S.; Cespi, M.; Casettari, L. Microfluidics for nanomedicines manufacturing: An affordable and low-cost 3D printing approach. *Int. J. Pharm.* **2021**, *599*, 120464. [CrossRef] [PubMed]
9. Camarillo-Escobedo, R.M.; Flores-Nuñez, J.L.; Garcia-Torales, G.; Hernandez-Campos, E.; Camarillo-Escobedo, J.M. 3D printed opto-microfluidic autonomous analyzer for photometric applications. *Sens. Actuators A Phys.* **2022**, *337*, 113425. [CrossRef]
10. Gong, H.; Woolley, A.T.; Nordin, G.P. High density 3D printed microfluidic valves, pumps, and multiplexers. *Lab Chip* **2016**, *16*, 2450–2458. [CrossRef] [PubMed]
11. Zhang, J.M.; Ji, Q.; Duan, H. Three-Dimensional Printed Devices in Droplet Microfluidics. *Micromachines* **2019**, *10*, 754. [CrossRef] [PubMed]
12. Zhang, J.; Xu, W.; Xu, F.; Lu, W.; Hu, L.; Zhou, J.; Zhang, C.; Jiang, Z. Microfluidic droplet formation in co-flow devices fabricated by micro 3D printing. *J. Food Eng.* **2021**, *290*, 110212. [CrossRef]
13. Ding, X.; Li, Z.; Liu, C. Monolithic, 3D-printed lab-on-disc platform for multiplexed molecular detection of SARS-CoV-2. *Sens. Actuators B Chem.* **2022**, *351*, 130998. [CrossRef] [PubMed]
14. Vangunten, M.T.; Walker, U.J.; Do, H.G.; Knust, K.N. 3D-Printed Microfluidics for Hands-On Undergraduate Laboratory Experiments. *J. Chem. Educ.* **2020**, *97*, 178–183. [CrossRef]

15. Hwang, Y.H.; Um, T.; Hong, J.; Ahn, G.N.; Qiao, J.; Kang, I.S.; Qi, L.; Lee, H.; Kim, D.P. Robust Production of Well-Controlled Microdroplets in a 3D-Printed Chimney-Shaped Milli-Fluidic Device. *Adv. Mater. Technol.* **2019**, *4*, 1900457. [CrossRef]
16. Song, R.; Abbasi, M.S.; Lee, J. Fabrication of 3D printed modular microfluidic system for generating and manipulating complex emulsion droplets. *Microfluid. Nanofluidics* **2019**, *23*, 92. [CrossRef]
17. Der, O.; Bertola, V. An experimental investigation of oil-water flow in a serpentine channel. *Int. J. Multiph. Flow* **2020**, *129*, 103327. [CrossRef]
18. Verma, R.K.; Ghosh, S. Effect of phase properties on liquid-liquid two-phase flow patterns and pressure drop in serpentine mini geometry. *Chem. Eng. J.* **2020**, *397*, 125443. [CrossRef]
19. Deltombe, R.; Kubiak, K.J.; Bigerelle, M. How to select the most relevant 3D roughness parameters of a surface. *Scanning* **2014**, *36*, 150–160. [CrossRef] [PubMed]
20. Kabir, H.; Garg, N. Rapid prediction of cementitious initial sorptivity via surface wettability. *npj Mater. Degrad.* **2023**, *7*, 52. [CrossRef]

Disclaimer/Publisher's Note: The statements, opinions and data contained in all publications are solely those of the individual author(s) and contributor(s) and not of MDPI and/or the editor(s). MDPI and/or the editor(s) disclaim responsibility for any injury to people or property resulting from any ideas, methods, instructions or products referred to in the content.